Pressure drop evaluation based on two-phase flow observation in packed bed system

AUTHOR(S):

Yasugi, Noriaki; Odaira, Naoya; Ito, Daisuke; Ito, Kei; Saito, Yasushi

CITATION:

Yasugi, Noriaki ...[et al]. Pressure drop evaluation based on two-phase flow observation in packed bed system. Mechanical Engineering Journal 2022, 9(4): 21-00437.

ISSUE DATE:

2022

URL:

http://hdl.handle.net/2433/279239

Bulletin of the JSME Vol.9, No.4, 2022
Mechanical Engineering Journal

Pressure drop evaluation based on two-phase flow observation in packed bed system

Noriaki YASUGI*, Naoya ODAIRA**, Daisuke ITO**, Kei ITO** and Yasushi SAITO**
* Graduate School of Energy Science, Kyoto University
Yoshida-Honmachi, Sakyo-ku, Kyoto, 606-8501, Japan
** Institute for Integrated Radiation and Nuclear Science, Kyoto University
2, Asashiro-Nishi, Kumatori-cho, Sennan-gun, Osaka, 590-0494, Japan
E-mail: ito.daisuke.5a@kyoto-u.ac.jp

Received: 24 December 2021; Revised: 24 June 2022; Accepted: 26 July 2022

Abstract
Two-phase pressure drop in the debris has been studied by many researchers concerning the debris cooling characteristics during a severe accident in a nuclear reactor. However, its flow regime transition of the two-phase flow in the debris has not been well understood, which strongly affects the interfacial drag and the pressure drop. Conventional models for gas-liquid two-phase flow pressure drop have not been established to evaluate interfacial drag accurately. In this study, high-speed imaging of a two-dimensional network model was performed to clarify the effect of flow patterns on interfacial drag and pressure drop. Usually, it would not be easy to visualize such two-phase flow behavior in a randomly packed bed due to the reflection/refraction of light and/or overlapping bubbles, even if the test section is made of transparent materials. Therefore, in this study, a test section, which simulates a two-dimensional network of porous structures, was fabricated to avoid overlapping bubbles. The two-phase flow pattern in the porous structure has been identified by high-speed imaging of the two-dimensional network model. The flow regime map based on the flow pattern visualization results is applied to the pressure drop evaluation and it could reduce the overestimation of experimental values. The experimental results suggested that the interfacial drag term should be modified in the gas-liquid two-phase flow pressure drop model.

Keywords : Two phase flow, Packed bed of spheres, Flow visualization, Flow regime map, Pressure drop

1. Introduction

In a severe accident of a nuclear reactor, the cooling characteristics of fuel debris are an essential factor for detailed accident simulation. Many studies have been conducted on debris cooling so far, and evaluation has been performed experimentally and analytically. In particular, research on the gas-liquid two-phase flow in the packed bed of spheres has been actively conducted to simulate the flow in fuel debris. The study of the flow structure and heat transfer characteristic of the two-phase flow in the packed bed is critical in severe accidents.

To predict two-phase flow in the packed bed, Lipinski (1982) proposed a two-phase pressure drop prediction model based on Ergun's equation for single-phase flow pressure drop prediction (Ergun, 1952). In addition, Reed (1991) and Hu & Theofanous (1991) improved the prediction accuracy by modifying the relative permeability and passability in the Lipinski model. In the Lipinski model, however, the interaction between gas and liquid is involved as the coefficients in the relative permeability and passability. So, Schulenberg & Müller (1987) added an interfacial drag term to the Lipinski model to consider the interfacial drag directly. Tung & Dhir (1988) proposed the interfacial drag equation for each flow pattern and enhanced the prediction accuracy of the pressure drop in the packed bed. Schmidt (2007) also modified the flow pattern transition criteria in Tung & Dhir's method. It has been reported that the interfacial drag term model gives better results than the experimental data of other researchers (Li et al., 2017, 2018). They identified the flow pattern in the packed bed of spheres by using the packed particle size and the void fraction. However, the void fraction is not a relevant experimental parameter, and the applicability of their flow pattern transitions to the wide flow conditions has

Paper No.21-00437
J-STAGE Advance Publication date : 4 August, 2022
[DOI: 10.1299/mej.21-00437]

not been investigated. Therefore, it is necessary to develop a flow regime map by observing the flow inside the packed bed for the prediction under a wide range of flow conditions. In general, the flow pattern of two-phase flow in a normal pipe is classified by the superficial gas and liquid velocity, as seen in the Mishima-Ishii flow regime map (Mishima and Ishi, 1984). Thus, the flow regime map for two-phase flow in the packed bed of spheres would help modify the interfacial drag term and enhance the pressure drop prediction accuracy.

This study aims to investigate the flow transition criteria to improve the accuracy of the pressure drop prediction. Because it is difficult to visualize the flow inside the packed bed and to identify the flow pattern, a quasi-two-dimensional packed bed test section (quasi-2D test section) simulates the uniformly packed bed of spheres with the same particle size is made for flow visualization. The pressure drop in this test section is also measured and compared with the prediction models such as the Lipinski model, and their applicability to present experimental results are clarified. The visualization results are compared with the existing flow regime maps of gas-liquid two-phase flow. Finally, the effect of the flow regime map on the pressure drop prediction is investigated.

Nomenclature

d_p	[m]	Packed particle size
F	[N/m^3]	Interfacial drag force
g	[m/s^2]	Gravitational acceleration
H_t	[m]	Distance of pressure drop measurement
j	[m/s]	Superficial velocity
k	[-]	Permeability
Q	[L/min]	Volumetric flow rate
v	[m/s]	Cross-sectional average velocity
ΔP	[Pa]	Pressure drop
P^*	[-]	Dimensionless pressure drop
α	[-]	Void fraction
ε	[-]	Porosity
η	[-]	Passability
μ	[kg/m s]	Viscosity
ρ	[kg/m^3]	Density
σ	[N/m]	Surface tension

subscripts

L	Liquid phase
G	Gas phase
i	Interface

2. Experiments

2.1 Quasi-2D test section for visualization

Observing the two-phase flow from outside the packed bed of spheres makes it challenging to accurately visualize the bubble behavior inside the packed bed due to the reflection/refraction of light and/or overlapping bubbles. Therefore, a quasi-two-dimensional flow path network is formed by avoiding the overlap of the flow channel in the direction of the observation. In a packed bed of spheres, the flow path through a hexagonal closest packed structure consists of minimum flow path units, as shown in Fig. 1. Two acrylic plates with semispherical (d_p = 10 mm) protrusion surfaces are manufactured to arrange the flow path unit quasi-two-dimensionally. The machined tool mark on the hemispheres is reduced for clear visualization by using an abrasive compound for acrylic resin. Those plates facing each other are fixed, as shown in Fig. 2, and a quasi-2D test section is prepared. The semispherical protrusion in each plate is located in a staggered arrangement. The hemispheres were in contact with the next spheres and the hemispheres were on another plate if those plates faced each other. The size of the semispherical protrusion area is 200 mm × 30 mm (height × width).

[DOI: 10.1299/mej.21-00437]

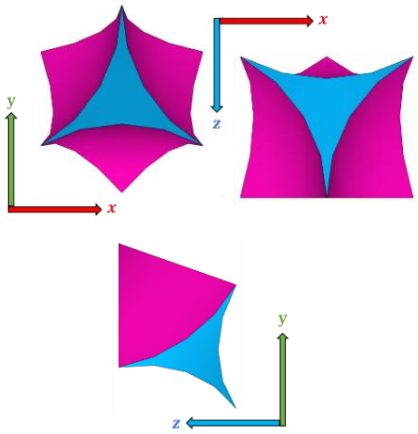

Fig. 1 The minimum flow path unit of hexagonal closest packed structure (Pink: Surface of the sphere, Blue: Flow channel cross-section).

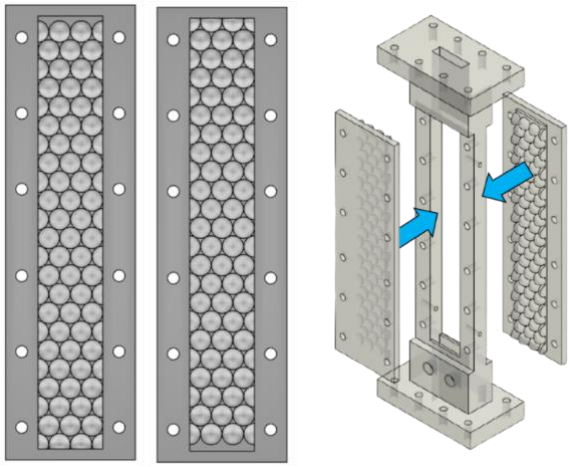

Fig. 2 Quasi-2D test section for two-phase flow visualization.

2.2 Experimental setup and method

Figure 3 shows a schematic diagram of the experimental setup for the two-phase flow visualization using the quasi-2D test section. The working fluids are air and tap water. Water is circulated by a pump and flows into the test section. Water temperature is measured by a thermocouple installed at the inlet of the test section. The temperature range during the experiments is from 26 to 31 °C. The density and viscosity are evaluated from the measured temperature. Air from a compressor is dried by an air dryer. Then, the compressed air is injected into the test section from three holes placed on the wall upstream of the packed section. The diameter of the holes is 1 mm. The two-phase mixture passed through the test section is separated at the upper tank and only water returns to the storage tank. In the liquid flow rate measurement, two float type flowmeters (KOFLOC, RK1250 series, 0.02 ~ 0.2 L/min and 0.1 ~ 1.0 L/min) and a digital flowmeter (KEYENCE, FD-P05, 0 ~ 5 L/min) are used. Table 1 shows the measurable ranges and calibration errors of these flowmeters. The calibration errors in Table 1 are the maximum errors between the calibration points and the calibration lines obtained by fitting them. Three types of mass flow meters with different ranges were used for gas flow rate measurement. The maximum measurable values are 1 L/min, 10 L/min, and 100 L/min, respectively. Their measurement errors are within ±3% of the full scales.

Three differential pressure sensors with a built-in amplifier were installed in the test section for the pressure drop measurement, as shown in Fig. 3. The distance between the differential pressure taps is 150 mm, and the difference in the pressures is measured through connected thin tubes to the side surfaces of the quasi-2D test section. The measurement ranges of the sensors are 0 to 10 kPa (COPAL, PA838-101D), 0 to 50 kPa (COPAL, PA838-501D), and 0 to 100 kPa (COPAL, PA838-102D), respectively. The measurement error of each sensor is approximately 0.5% of the full scale. Differential pressure measurement is performed by using all sensors with a sampling rate of 300 Hz. The measurement time is 10 s, and the averaged value is calculated by data processing and used to evaluate the pressure drop. Some factors like hysteresis, temperature characteristics, offset, and so on can be considered as the uncertainty of the differential pressure gauge. The sensor involves a hysteresis error of ±0.5% and temperature characteristics of ±0.1% in full scale. In addition, calibration is performed in advance, and the differential pressure is calculated using the calibration curve. The error at that time was less than ±0.1%. It was confirmed that the error obtained from the calibration was sufficiently small compared to the accuracy of the equipment specifications. An absolute pressure gauge is used to correct the superficial gas velocity in the test section. The pressure at the center of the test section is estimated from the measured absolute pressure and differential pressure, and the superficial gas velocity is calculated.

The observation of the flow structure and pattern in air-water two-phase flow in the test section is performed using a high-speed camera (IDT, Motion Pro Y4-lite). The imaging area is the center of the packed section. The frame rate is 1000 frames/s. The exposure time is set at 10 μs to obtain appropriate gray value images, and 1000 images were recorded to evaluate flow patterns.

[DOI: 10.1299/mej.21-00437]

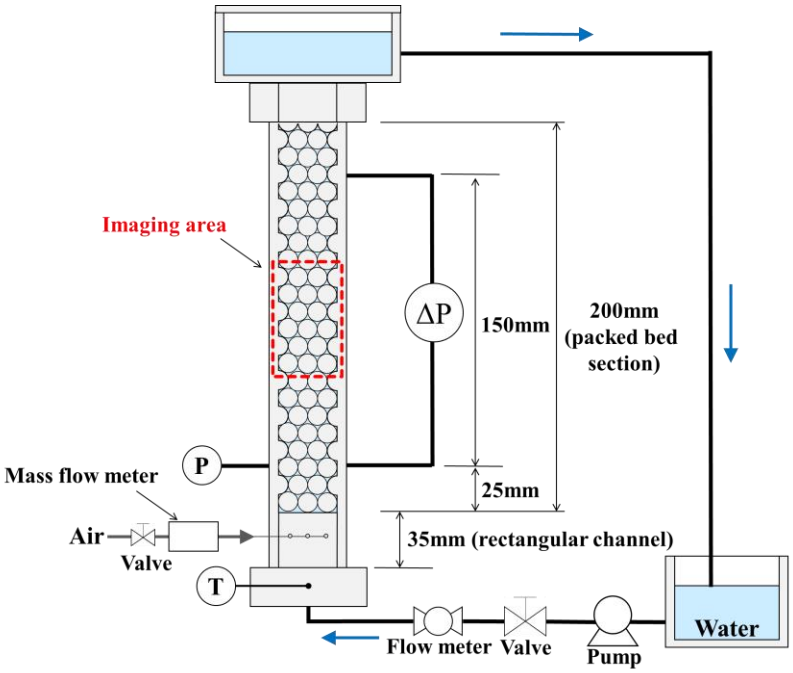

Fig. 3 Schematic diagram of experimental apparatus with the quasi-2D test section.

Table 1 Measurable ranges and calibration errors of water flow meters.

Water flow meters	Used range [L/min]	Calibration error
RK1250 (0.2 L/min)	$0 < Q_L \leq 0.2$	± 2.4%
RK1250 (1 L/min)	$0.2 < Q_L \leq 1.0$	± 2.1%
FD-P05	$1.0 < Q_L \leq 2.2$	± 2.3%

3. Results and discussion

3.1 Pressure drop measurement in single-phase flow

As the first step, the pressure drop characteristics in a single-phase water flow were measured in the quasi-2D test section. The porosity of the present test section is estimated by comparing the measured pressure drop with that calculated by the Ergun equation, which can predict a single-phase pressure drop in the packed bed of spheres. Ergun equation is as follows (Ergun, 1952):

$$\frac{\Delta P}{H_t} = \rho g + \frac{150\mu v\,(1-\varepsilon)^2}{\varepsilon^3 {d_p}^2} + \frac{1.75(1-\varepsilon)\rho v^2}{\varepsilon^3 d_p} \tag{1}$$

The measured results are shown in Fig. 4. The pressure drop increases with the liquid velocity. The standard deviation at the averaged pressure drop value was less than 0.15 kPa. This result agrees well with the Ergun equation when the porosity value of 0.258 is employed in the Ergun equation. The coefficient of determination in this fitting is 0.996. From this, it can be anticipated that the porosity of the quasi-2D test section is 0.258. The porosity of the hexagonal closest packed structure is calculated theoretically as 0.260. The estimated porosity by the Ergun equation shows a lower value. This might be attributed to the machining accuracy and error in assembling the test section. The value 0.258 is used for pressure drop evaluation.

[DOI: 10.1299/mej.21-00437]

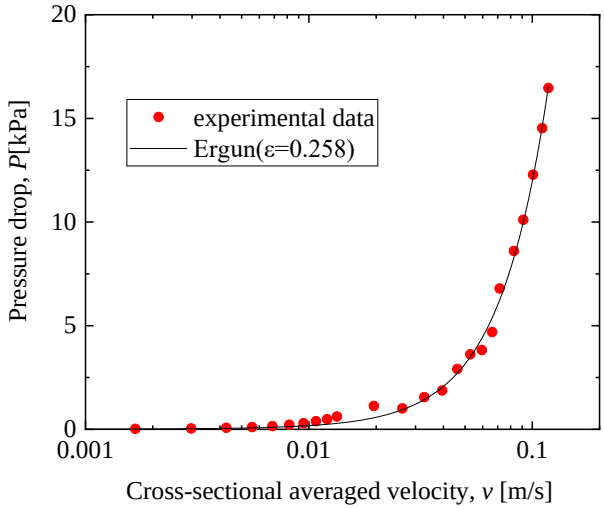

Fig. 4 Comparison of pressure drop measurement data and Ergun model prediction for single-phase flow.

3.2 Pressure drop measurement in two-phase flow

Pressure drops under two-phase flow conditions are measured, and the results are shown in Fig. 5. In this figure, the horizontal axis denotes the superficial gas velocity, and the vertical axis denotes the dimensionless pressure drop. Here, the dimensionless pressure drop is defined as follows (Tung and Dhir, 1988):

$$P^* = \frac{\Delta P / H_t}{g(\rho_L - \rho_G)} \tag{2}$$

As the superficial gas velocity increases, the pressure drop increases gradually at $j_G < 0.1$ m/s and rapidly at $j_G > 0.1$ m/s, where the inertial loss term effect might be dominant.

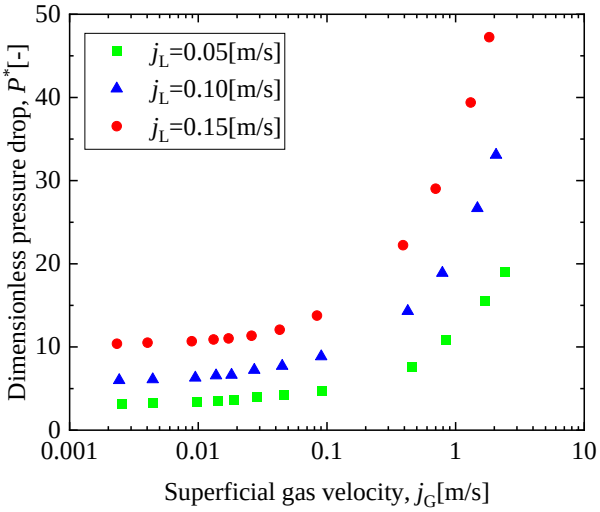

Fig. 5 Variation of dimensionless pressure drop with superficial gas velocity.

Next, the measured pressure drop is compared with the Lipinski model, as represented by the following equations proposed by Lipinski (1982).

$$\frac{\Delta P_L}{H_t} = \rho_L g + \frac{150\mu_L v_L (1-\varepsilon)^2}{k_L \varepsilon^3 {d_p}^2} + \frac{1.75(1-\varepsilon)\rho_L v_L^2}{\eta_L \varepsilon^3 d_p} \tag{3}$$

[DOI: 10.1299/mej.21-00437]

$$\frac{\Delta P_G}{H_t} = \rho_G g + \frac{150\mu_G v_G (1-\varepsilon)^2}{k_G \varepsilon^3 {d_p}^2} + \frac{1.75(1-\varepsilon)\rho_G v_G^2}{\eta_G \varepsilon^3 d_p} \tag{4}$$

Here, $\Delta P = \Delta P_L = \Delta P_G$. Eqs. (3) and (4) include relative passability k and relative permeability η which is a function of void fraction and liquid saturation. The relative permeability is the measure of the flow conductance, and the relative permeability is a turbulent counterpart of the relative passability. These parameters are proposed by many researchers, Lipinski (1982), Reed (1991), and Hu & Theofanous (1991), and each researcher proposed different correlations. Table 2 shows their formulas for relative passability and relative permeability. Thus, we compared measured data of pressure drop and each model in Table 2. In addition to the abovementioned parameters, some researchers proposed an additional term named interfacial drag term was added in Eq. (3) and (4) as follows:

$$\frac{\Delta P_L}{H_t} = \rho_L g + \frac{150\mu_L v_L (1-\varepsilon)^2}{k_L \varepsilon^3 {d_p}^2} + \frac{1.75(1-\varepsilon)\rho_L v_L^2}{\eta_L \varepsilon^3 d_p} - \frac{F_i}{1-\alpha} \tag{5}$$

$$\frac{\Delta P_G}{H_t} = \rho_G g + \frac{150\mu_G v_G (1-\varepsilon)^2}{k_G \varepsilon^3 {d_p}^2} + \frac{1.75(1-\varepsilon)\rho_G v_G^2}{\eta_G \varepsilon^3 d_p} + \frac{F_i}{\alpha} \tag{6}$$

The interfacial drag force F_i is proposed by Schulenberg & Müller (1987) and Tung & Dhir (1988). F_i proposed by Schulenberg & Müller is a function of void fraction. On the other hand, F_i proposed by Tung & Dhir is given for each flow pattern based on the flow transition criteria shown in Table 3. The criteria are determined by the void fraction.

Table 2 Calculation formula for relative passability and relative permeability.

Model	k_L	η_L	k_G	η_G	F_i
Lipinski (1982)	$(1-\alpha)^3$	$(1-\alpha)^3$	α^3	α^3	-
Reed (1991)	$(1-\alpha)^3$	$(1-\alpha)^5$	α^3	α^5	-
Hu & Theofanous (1991)	$(1-\alpha)^3$	$(1-\alpha)^6$	α^3	α^6	-
Schulenberg & Műller (1987)	$(1-\alpha)^3$	$(1-\alpha)^5$	α^3	α^6, $\alpha > 0.3$; $0.1\alpha^4$, $\alpha < 0.3$	○
Tung & Dhir (1988)	$(1-\alpha)^3$	$(1-\alpha)^3$	$\left(\frac{1-\varepsilon}{1-\varepsilon\alpha}\right)^{\frac{4}{3}}\alpha^3$	$\left(\frac{1-\varepsilon}{1-\varepsilon\alpha}\right)^{\frac{4}{3}}\alpha^3$	○

Table 3 Flow pattern ranges in Tung & Dhir model.

Ranges of void fraction	Formula	Flow Patterns
$0 \le \alpha < \alpha_1$	$\alpha_1 = \min(0.3,\ 0.6(1-D_b/d_p)^2)$ $(D_b = \sqrt{\sigma/\{g(\rho_L-\rho_G)\}})$	Bubbly flow
$\alpha_1 \le \alpha < \alpha_2$	$\alpha_2 = \pi/6$	Transition
$\alpha_2 \le \alpha < \alpha_3$	$\alpha_3 = 0.6$	Slug flow
$\alpha_3 \le \alpha < \alpha_4$	$\alpha_4 = \pi\sqrt{2}/6$	Transition
$\alpha_4 \le \alpha \le 1$		Annular flow

[DOI: 10.1299/mej.21-00437]

Figures 6 and 7 show the comparison of measured data and model calculation results of pressure drop. Figure 6 is for models which don't include interfacial drag and Figure 7 is for models which include interfacial drag. As a result, the Lipinski model shows the best agreement with the measured values among all employed models in the present system. In the prediction results of the model with interfacial drag, Tung & Dhir's model, which directly considers the interfacial drag effect, represents a closer result to measured data than Schulenberg & Mueller's model. However, they are worse than the Lipinski model. Generally, it is expected that the models with the interfacial drag term show good prediction accuracy, as reported in the previous studies (Li et al., 2017, 2018, Park et al., 2018). The present packed bed system has mono-sized spherical particles, and they are regularly packed. Also, the flow path is arranged two-dimensionally, because of the flow visualization. Therefore, the tendency of the pressure drop prediction is different for randomly packed beds, and the Lipinski model shows good results. However, it is difficult for the Lipinski model to extend the applicable range (wide flow conditions, different particle shape, size, etc.) because the parameters are less than Tung & Dhir's model. So, the effect of the interfacial drag term on prediction accuracy should be studied. In this study, the possibility of improvement of the prediction accuracy is investigated by using Tung & Dhir's model and the flow observation results.

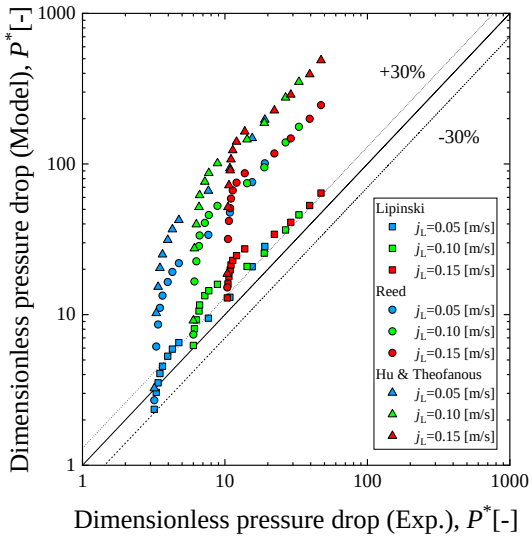

Fig. 6 Comparison of dimensionless pressure drop measurement data and model predictions without interfacial drag.

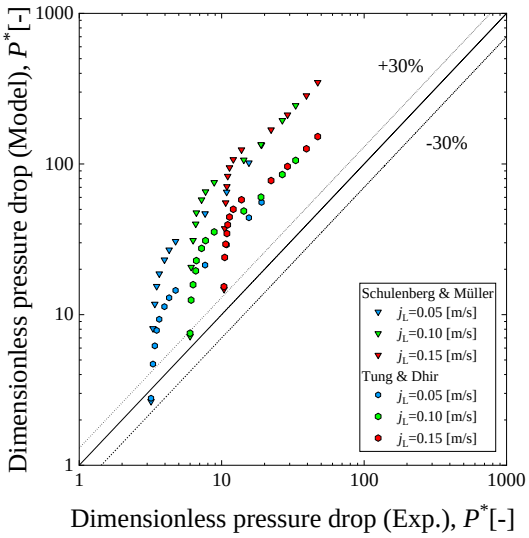

Fig. 7 Comparison of dimensionless pressure drop measurement data and model predictions with interfacial drag.

3.3 Visualization and flow regime identification

Two-phase flow behavior in the quasi-2D test section is observed by the high-speed camera. The acquired images in single-phase and bubbly flow are shown in Fig.8 (a) and (b), respectively. As you can see, Figure 8 (b) is difficult to observe bubbles in the two-phase flow because of the experimental apparatus. Thus, the two-phase flow images are normalized by a liquid phase image for precise observation of bubbles, as shown in Fig. 8 (c). This normalization can eliminate the structure of the flow channel. Following two-phase flow images were normalized by this procedure.

The typical images for bubbly, slug, and annular flows are shown in Fig. 9. Bubbles are relatively small and spherical in the bubbly flow images in Fig. 9 (a). Those bubbles pass through the gaps between the spheres. As the superficial gas velocity increases, the flow becomes slug flow, and the bubbles are extended to cover the cross-section of the flow path, as shown in Fig. 9 (b). Figure 9 (c) shows typical images of annular flow. As mentioned above, all images shown in Fig. 9 are normalized by water single-phase flow image. However, the flow path structure is visible in Fig.9(c). It is because the gas-liquid interface covers the entire flow path in annular flow. As a result, the flow regime can be easily observed from these images using the quasi-2D test section.

[DOI: 10.1299/mej.21-00437]

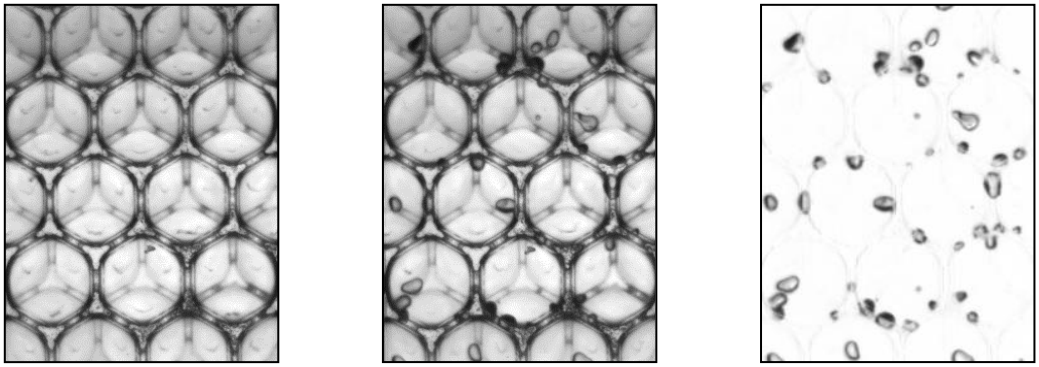

(a) Single-phase flow (b) Bubbly flow (c) Normalized image

Fig. 8 Air-water two-phase flow images.

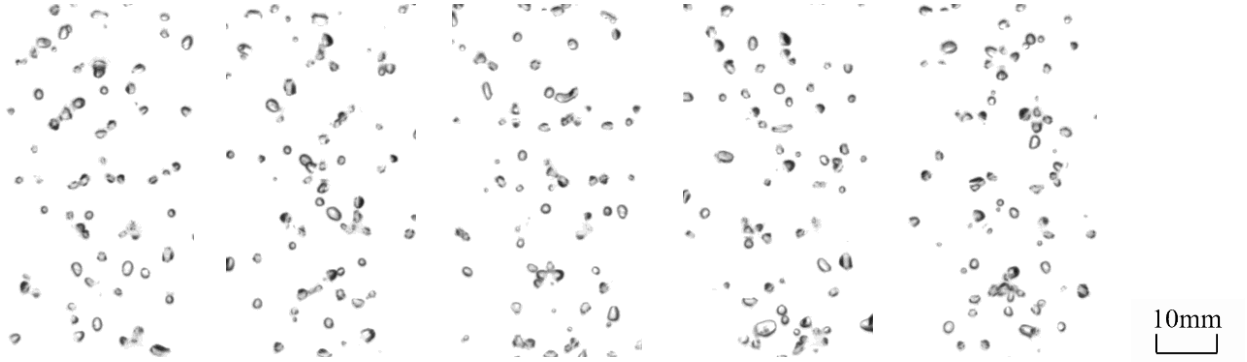

(i) 0 ms (ii) 20 ms (iii) 40 ms (iv) 60 ms (v) 80 ms

(a) Bubbly flow, j_L=0.05 m/s, j_G=0.003 m/s

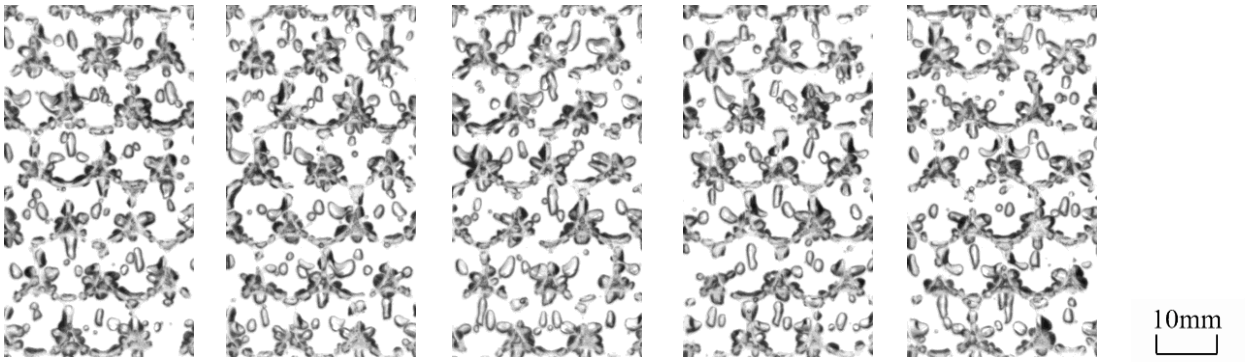

(i) 0 ms (ii) 20 ms (iii) 40 ms (iv) 60 ms (v) 80 ms

(b) Slug flow, j_L=0.05 m/s, j_G=0.02 m/s

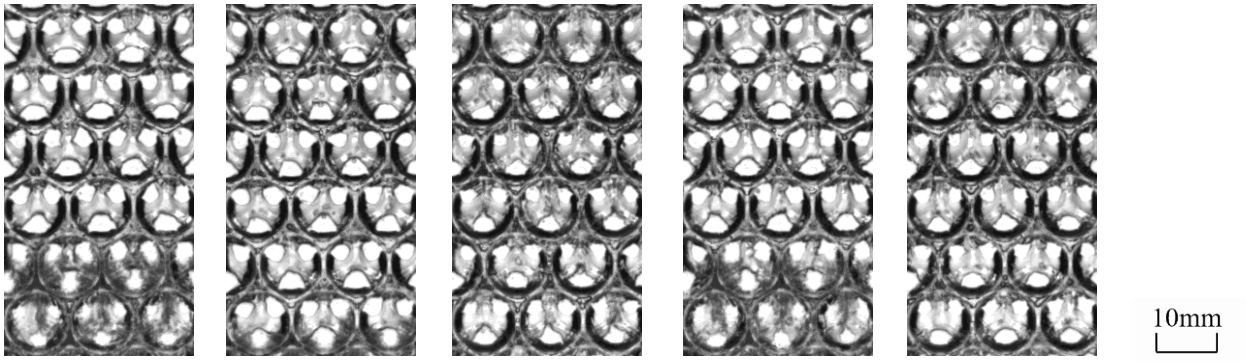

(i) 0 ms (ii) 20 ms (iii) 40 ms (iv) 60 ms (v) 80 ms

(c) Annular flow, j_L=0.05 m/s, j_G=2.0 m/s

Fig. 9 High-speed camera observation of two-phase flow pattern.

[DOI: 10.1299/mej.21-00437]

From the flow visualization results, the flow pattern of the gas-liquid two-phase flow in the quasi-2D test section is determined and summarized by the superficial gas and liquid velocity, as shown in Fig. 10. The vertical axis denotes the superficial liquid velocity j_L, and the horizontal axis denotes the superficial gas velocity j_G. The solid line in the figure represents the flow transition criteria proposed for the two-phase flow in an ordinary diameter circular tube by Mishima-Ishii (1984) and the dashed line represents the criteria for the narrow gap rectangular channel proposed by Hibiki-Mishima (2001). In the calculations of both flow transition criteria, the equivalent diameter of the flow channel in the visualization experiment was assumed to be 1.88 mm based on the averaged hydraulic diameter in the minimum flow path unit shown in Fig. 1. In Fig.10, the transition from bubbly to slug flow in Hibiki-Mishima (H-M) map occurs at lower j_G than Mishima-Ishii (M-I) map, because the bubble coalescence is accelerated due to the narrow flow path. The experimental results also show the transition at low j_G. On the other hand, the transition from slug to annular flow represents an opposite trend. The transition in H-M map occurs at higher j_G than M-I map. In the packed bed system, the confined flow channel suppresses the formation of the liquid film in the annular flow, and the observation results of the flow pattern show good agreement with H-M map. Previously, Tung & Dhir (1988) and Schumidt (2007) used the flow pattern transition criteria classified by a void fraction and particle size, and the pressure drop was evaluated. However, the flow regime is varied significantly by the superficial gas and liquid velocities despite the same particle size, as shown in this result. Thus, it is difficult to classify the flow pattern from only the void fraction. Consequently, detailed consideration of the flow pattern in the packed bed is very important to improve the pressure drop evaluation.

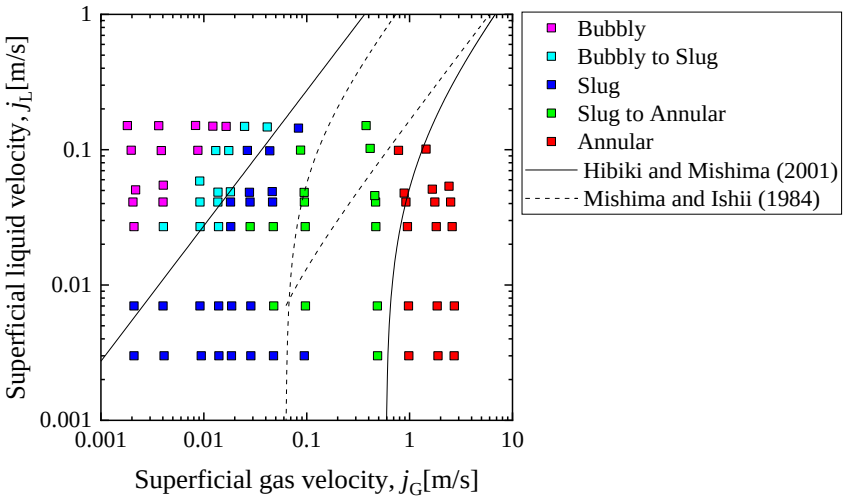

Fig. 10 Comparison of observed flow patterns with existing flow regime maps of gas-liquid two-phase flow.

Figure 11 compares pressure drops between the calculated values and the experimental data. In these figures, the plot of Tung & Dhir indicates the pressure drop calculated with Tung & Dhir interfacial drag calculation based on the flow regime map identified only by the void fraction value. On the other hand, the plot of Tung & Dhir (Observed flow regime) also employs Tung & Dhir interfacial drag calculation, though the flow regime transition is determined by the obtained experimental results as shown in Fig. 10. In each graph, the horizontal axis denotes the pressure drop per unit height measured in the experiment, and the vertical axis denotes that of calculation results. The results are shown under three superficial liquid velocity conditions, i.e. j_L = 0.05, 0.10, and 0.15 m/s. On the lower superficial liquid and gas velocity condition which means a lower pressure drop condition ($\Delta P/H_t < 0.3$), the model calculation result indicates values close to the present experimental data. As to increase superficial liquid and gas velocity which means increasing pressure drop, the model calculation result becomes to overestimate the present experimental result. From those results, we considered that overestimation of pressure drop may be caused by a discrepancy of flow patterns between the model and the present result because interfacial drag is chosen from flow patterns. Flow patterns in the model are determined by a void fraction, however, flow patterns in a packed bed system are hardly observed especially in the center of the system and our quasi-2D test section can observe flow patterns clearly. In addition, recent studies claimed that the interfacial drag term in Tung & Dhir model overestimates the pressure drop, particularly for annular flow (Taherzadeh and Saidi, 2015; Park et al., 2018). Thus, we employed interfacial drag corresponding to observed flow patterns, not

[DOI: 10.1299/mej.21-00437]

flow patterns determined by void fraction as proposed by Tung & Dhir. It is obvious that overestimated value approaches their experimental values in most cases by employing the experimentally obtained flow regime map. The evaluation accuracy can be improved by considering the appropriate flow regime for each flow condition. It should be noted here that the discrepancy of the pressure drop between the calculated values and experimental data tends to increase with the increase in the pressure drop value. The interfacial drag term will be improved to address this problem in future work.

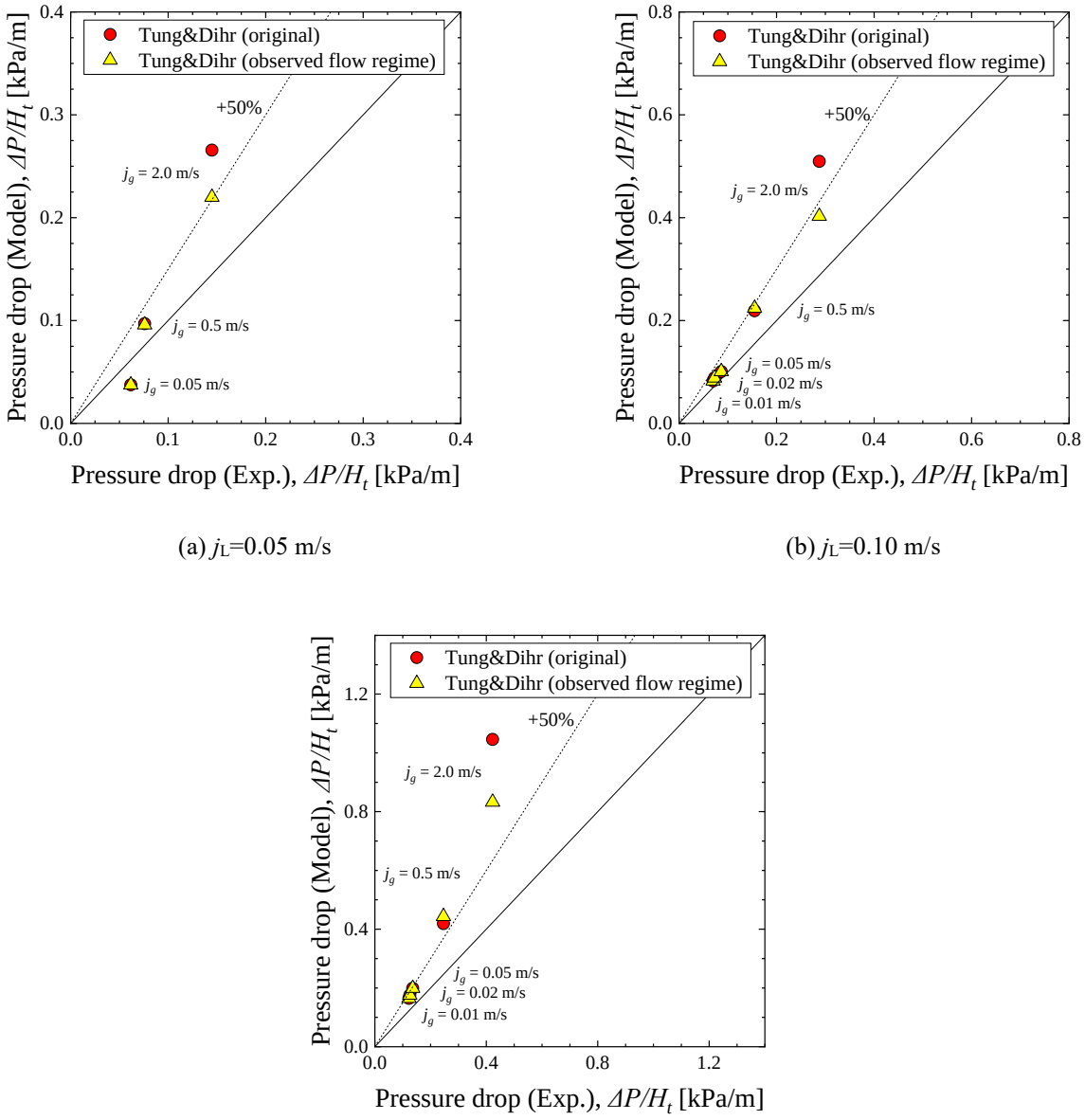

(a) j_L=0.05 m/s

(b) j_L=0.10 m/s

(c) j_L=0.15 m/s

Fig. 11 Comparison of Tung & Dhir model with modified flow regime from visualization results and pressure drop experimental values.

4. Conclusion

The pressure drop measurement and flow visualization in the packed bed of spheres were performed using a quasi-2D test section which simulates the uniformly packed bed with the same particle size. The measured pressure drop was compared with the Lipinski-type models. Although the experimental results agreed with the Lipinski model in the present test section, the effect of the interfacial drag should be investigated to extend the applicability of such model.

[DOI: 10.1299/mej.21-00437]

The two-phase flow regime transition was investigated by visualizing the flow structure in the test section. The observed flow pattern was compared with the existing flow regime maps and well correlated with Hibiki-Misihma (2001) map for narrow rectangular channels when the averaged hydraulic diameter expresses the equivalent diameter in the minimum flow path unit in the test section. The previous flow transition criteria of the packed bed were classified by the void fraction and packed particle size. However, the flow regime map obtained in this study is extremely useful to understand the flow in the sphere-packed bed. In addition, the flow pattern transition criteria in the interfacial drag term of Tung & Dhir's model were modified based on the flow pattern visualization results, and the enhancement of the prediction accuracy was confirmed.

In this study, the present test section is a simplified packed bed system, which has mono-sized spherical particles and a regular arrangement. The effect of the flow regime transition should be investigated for different particle sizes. In addition, the void fraction measurement in the packed bed is required to compare the flow regime with Tung & Dhir's transition criteria.

References

Ergun, S., Fluid flow through packed columns, Chemical Engineering Progress, Vol.48, (1952), pp.89-94.

Hibiki, T. and Mishima, K., Flow regime transition criteria for upward two-phase flow in vertical narrow rectangular channels, Nuclear Engineering and Design, Vol.203, (2001), pp.117-131.

Hu, K., and Theofanous, T. G., On the measurement and mechanism of dry-out in volumetrically heated coarse particle beds, International Journal of Multiphase Flow, Vol.17, No.4, (1991), pp.519-532.

Li, L., Kong, L., Zou, X., and Wang, H., Pressure losses and interfacial drag for two-phase flow in porous beds with coarse particles, Annals of Nuclear Energy, Vol.101, (2017), pp.481-488.

Li, L., Wang, K., Zhang, S. and Lei, X., An experimental study on two-phase flow resistances and interfacial drag in packed porous beds, Nuclear Engineering and Technology, Vol.50, (2018), pp.842-848.

Lipinski, R. J., A model for boiling and dryout in particle beds, Sandia National Labs Report, NUREG/CR-2646 (1982).

Mishima, K. and Ishii, M., Flow regime transition criteria for upward two-phase flow in vertical tubes, International Journal of Heat and Mass Transfer, Vol.27, No.5, (1984), pp.723-737.

Park, J. H., Park, H. S., Lee, M. and Moriyama, K., Modeling of pressure drop in two-phase flow of mono-sized spherical particle beds, International Journal Heat and Mass Transfer, Vol.127, (2018), 986–995.

Reed, A. W., The effect of channeling on the dry-out of heated particulate beds immersed in a liquid pool, PhD thesis, Massachusetts Institute of Technology, Cambridge (1991).

Schmidt, W., Interfacial drag of two-phase flow in porous media, International Journal of Multiphase Flow, Vol.33, (2007), pp.638–657.

Schulenberg, T. and Müller, U., An improved model for two-phase flow through beds of coarse particles, International Journal of Multiphase Flow, Vol.13, (1987), pp.87–97.

Taherzadeh, M. and Saidi, M. S., Modeling of two-phase flow in porous media with heat generation, International Journal Multiphase Flow, Vol.69, (2015), pp.115–127.

Tung, V. X. and Dhir, V. K., A hydrodynamic model for two-phase flow through porous media, International Journal of Multiphase Flow, Vol.14, (1988), pp.47–65.

[DOI: 10.1299/mej.21-00437]